RANDOM MATRIX THEORY AND DIRAC SPECTRUM AT NONZERO TEMPERATURE AND DENSITY

B.A. BERG
Department of Physics, The Florida State University, Tallahassee, FL 32306, USA

H. MARKUM AND R. PULLIRSCH
Institut für Kernphysik, Technische Universität Wien, A-1040 Vienna, Austria

AND

T. WETTIG
Department of Physics, Yale University, New Haven, CT 06520-8120, USA

We investigate the eigenvalue spectrum of the staggered Dirac matrix in SU(3) gauge theory and in full QCD as well as in quenched U(1) theory on various lattice sizes. As a measure of the fluctuation properties of the eigenvalues, we study the nearest-neighbor spacing distribution, $P(s)$. We further study lattice QCD at nonzero chemical potential, μ, by constructing the spacing distribution of adjacent eigenvalues in the complex plane. We find that in all regions of their phase diagrams, compact lattice gauge theories have bulk spectral correlations given by random matrix theory, which is an indication for quantum chaos.

1. QCD at Nonzero Temperature

The properties of the eigenvalues of the Dirac operator are of great importance for the understanding of certain features of QCD. For example, the accumulation of small eigenvalues is, via the Banks-Casher formula [1], related to the spontaneous breaking of chiral symmetry. Recently, the fluctuation properties of the eigenvalues in the bulk of the spectrum have also attracted attention. It was shown in Ref. [2] that on the scale of the mean level spacing they are described by random matrix theory (RMT). In particular, the nearest-neighbor spacing distribution $P(s)$, i.e., the distribution of spacings s between adjacent eigenvalues on the unfolded scale, agrees with

the Wigner surmise of RMT. According to the Bohigas-Giannoni-Schmit conjecture [3], quantum systems whose classical counterparts are chaotic have a nearest-neighbor spacing distribution given by RMT whereas systems whose classical counterparts are integrable obey a Poisson distribution, $P_{\rm P}(s) = e^{-s}$. Therefore, the specific form of $P(s)$ is often taken as a criterion for the presence or absence of "quantum chaos".

In RMT, one has to distinguish several universality classes which are determined by the symmetries of the system. For the case of the QCD Dirac operator, this classification was done in Ref. [4]. Depending on the number of colors and the representation of the quarks, the Dirac operator is described by one of the three chiral ensembles of RMT. As far as the fluctuation properties in the bulk of the spectrum are concerned, the predictions of the chiral ensembles are identical to those of the ordinary ensembles [5]. In Ref. [2], the Dirac matrix was studied in SU(2) using both staggered and Wilson fermions which correspond to the chiral symplectic and orthogonal ensemble, respectively. Here [6], we study SU(3) with staggered fermions which corresponds to the chiral unitary ensemble. The RMT result for the nearest-neighbor spacing distribution can be expressed in terms of so-called prolate spheroidal functions, see Ref. [7]. A very good approximation to $P(s)$ is provided by the Wigner surmise for the unitary ensemble,

$$P_{\rm W}(s) = \frac{32}{\pi^2} s^2 e^{-4s^2/\pi} \; . \tag{1}$$

We generated gauge field configurations using the standard Wilson plaquette action for SU(3) with and without dynamical fermions in the Kogut-Susskind prescription. We have worked on a $6^3 \times 4$ lattice with various values of the inverse gauge coupling $\beta = 6/g^2$ both in the confinement and deconfinement phase. We typically produced 10 independent equilibrium configurations for each β. Because of the spectral ergodicity property of RMT one can replace ensemble averages by spectral averages if one is only interested in bulk properties.

The Dirac operator, $\not{D} = \not{\partial} + ig\not{A}$, is anti-hermitian so that all eigenvalues are imaginary. For convenience, we denote them by $i\lambda_n$ and refer to the λ_n as the eigenvalues. Because of $\{\not{D}, \gamma_5\} = 0$ the nonzero λ_n occur in pairs of opposite sign. All spectra were checked against the analytical sum rules $\sum_n \lambda_n = 0$ and $\sum_{\lambda_n > 0} \lambda_n^2 = 3V$, where V is the lattice volume. To construct the nearest-neighbor spacing distribution from the eigenvalues, one first has to "unfold" the spectra [7].

Figure 1 compares $P(s)$ of full QCD with $N_f = 3$ flavors and quark mass $ma = 0.05$ to the RMT result. In the confinement as well as in the deconfinement phase we observe agreement with RMT up to very high β (not shown). The observation that $P(s)$ is not influenced by the presence

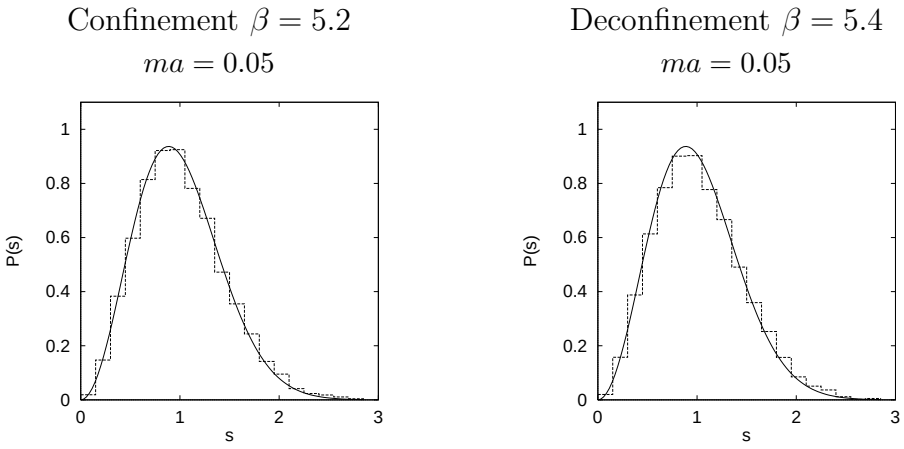

Figure 1. The nearest-neighbor spacing distribution $P(s)$ on a $6^3 \times 4$ lattice in full QCD (histograms) compared with the random matrix result (solid lines). There are no changes in $P(s)$ across the deconfinement phase transition.

of dynamical quarks could have been expected from the results of Ref. [5], which apply to the case of massless quarks. Our results, and those of [2], indicate that massive dynamical quarks do not affect $P(s)$ either.

No signs for a transition to Poisson regularity are found. The deconfinement phase transition does not seem to coincide with a transition in the spacing distribution. For very large values of β far into the deconfinement region, the eigenvalues start to approach the degenerate eigenvalues of the free theory, given by $\lambda^2 = \sum_{\mu=1}^{4} \sin^2(2\pi n_\mu / L_\mu)/a^2$, where a is the lattice constant, L_μ is the number of lattice sites in the μ-direction, and $n_\mu = 0, \ldots, L_\mu - 1$. In this case, the spacing distribution is neither Wigner nor Poisson. It is possible to lift the degeneracies of the free eigenvalues using an asymmetric lattice where L_x, L_y, etc. are relative primes and, for large lattices, the distribution is then Poisson, $P_{\rm P}(s) = e^{-s}$, see Fig. 2.

2. QCD at Nonzero Density

Physical systems which are described by non-hermitian operators have attracted a lot of attention recently, among others QCD at nonzero chemical potential μ [8]. There, the Dirac operator loses its hermiticity properties so that its eigenvalues become complex. The aim of the present analysis is to investigate whether non-hermitian RMT is able to describe the fluctuation properties of the complex eigenvalues of the QCD Dirac operator. The eigenvalues are generated on the lattice for various values of μ. We apply a two-dimensional unfolding procedure to separate the average eigenvalue

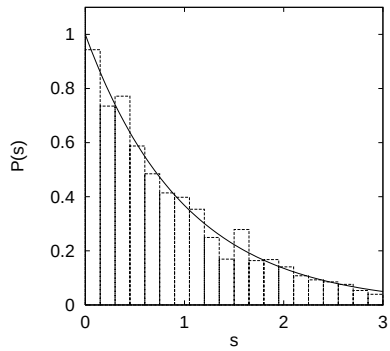

Figure 2. Nearest-neighbor spacing distribution $P(s)$ for the free Dirac operator on a $53 \times 47 \times 43 \times 41$ lattice compared with a Poisson distribution, e^{-s}.

density from the fluctuations and construct the nearest-neighbor spacing distribution, $P(s)$, of adjacent eigenvalues in the complex plane. The data are then compared to analytical predictions of non-hermitian RMT.

We start with a few definitions. A formulation of the QCD Dirac operator at $\mu \neq 0$ on the lattice in the staggered scheme is given by [9]

$$\begin{aligned} M_{x,y}(U,\mu) &= \frac{1}{2a}\sum_{\nu=\hat{x},\hat{y},\hat{z}}[U_\nu(x)\eta_\nu(x)\delta_{y,x+\nu} - \text{h.c.}] \\ &\quad + \frac{1}{2a}\left[U_{\hat{t}}(x)\eta_{\hat{t}}(x)e^{\mu}\delta_{y,x+\hat{t}} - U^\dagger_{\hat{t}}(y)\eta_{\hat{t}}(y)e^{-\mu}\delta_{y,x-\hat{t}}\right] \end{aligned} \quad (2)$$

with the link variables U and the staggered phases η.

We consider the gauge group SU(3) which corresponds to the symmetry class of the chiral unitary ensemble of RMT [4, 10]. At zero chemical potential, all Dirac eigenvalues are purely imaginary, and the nearest-neighbor spacing distribution, $P(s)$, of the lattice data agrees with the Wigner surmise of hermitian RMT, Eq. (1), both in the confinement and in the deconfinement phase (see Fig. 1). This finding implies strong correlations of the eigenvalues. For uncorrelated eigenvalues $P(s)$ is given by the Poisson distribution.

For a complex spectrum, we define $P(s)$ to represent the spacing distribution of nearest neighbors in the complex plane, i.e., for each eigenvalue z_0 one identifies the eigenvalue z_1 for which $s = |z_1 - z_0|$ is a minimum [11]. After ensemble averaging, one obtains a function $P(s, z_0)$ which, in general, depends on z_0. The dependence on z_0 can be eliminated by unfolding the spectrum, i.e., by applying a local rescaling of the energy scale so that the average spectral density is constant in a bounded region in the complex plane and zero outside [12]. After unfolding, a spectral average over z_0 yields $P(s)$.

For $\mu > 0$, the eigenvalues of the matrix in Eq. (2) move into the complex plane. If the real and imaginary parts of the strongly correlated eigenvalues have approximately the same average magnitude, the system should be described by the Ginibre ensemble of non-hermitian RMT [13]. In the Ginibre ensemble, the average spectral density is already constant inside a circle and zero outside, respectively. In this case, unfolding is not necessary, and $P(s)$ is given by [11]

$$P_{\rm G}(s) = c\, p(cs)\,, \quad p(s) = 2s \lim_{N\to\infty} \left[\prod_{n=1}^{N-1} e_n(s^2)\, e^{-s^2} \right] \sum_{n=1}^{N-1} \frac{s^{2n}}{n! e_n(s^2)}\,, \qquad (3)$$

where $e_n(x) = \sum_{m=0}^{n} x^m/m!$ and $c = \int_0^\infty ds\, s\, p(s) = 1.1429....$ This result holds for strongly non-hermitian matrices, i.e., for $\mathrm{Re}(z) \approx \mathrm{Im}(z)$ on average. In the regime of weak non-hermiticity [14], where the typical magnitude of the imaginary parts of the eigenvalues is equal to the mean spacing of the real parts, the RMT prediction deviates from Eq. (3). We shall comment on this regime below. For uncorrelated eigenvalues in the complex plane, the Poisson distribution becomes [11]

$$P_{\bar{\rm P}}(s) = \frac{\pi}{2}\, s\, e^{-\pi s^2/4}\,. \qquad (4)$$

This should not be confused with the Wigner distribution (1).

Our simulations were done with gauge group SU(3) on a $6^3 \times 4$ lattice using $\beta = 6/g^2 = 5.2$ in the confinement region and $\beta = 5.4$ in the deconfinement region for $N_f = 3$ flavors of staggered fermions of mass $ma = 0.1$. Despite major efforts [15] there is currently no feasible solution to the problem of a complex weight function in lattice simulations. (In a random matrix model, the numerical effort to generate a statistically significant ensemble of configurations including the complex Dirac determinant was shown to grow exponentially with $\mu^2 N$, where N is the lattice size [16].) Therefore, the gauge field configurations were generated at $\mu = 0$, and the chemical potential was added to the Dirac matrix afterwards. Both in the confinement and deconfinement, we sampled 50 independent configurations.

Typical eigenvalue spectra are shown in Fig. 3 for four different values of μ (in units of $1/a$) at $\beta = 5.2$. As expected, the size of the real parts of the eigenvalues grows with μ, consistent with Ref. [17]. Since the average spectral density is not constant, we have to apply the unfolding method defined in [12].

Our results for $P(s)$ are presented in Fig. 4. There are minor quantitative but no qualitative differences between confinement and deconfinement phase, which is consistent with our findings at $\mu = 0$ (see Fig. 1). As a function of μ, we expect to find a transition from Wigner to Ginibre behavior in $P(s)$, as is indeed seen in the figures. For $\mu = 0.1$, the data are

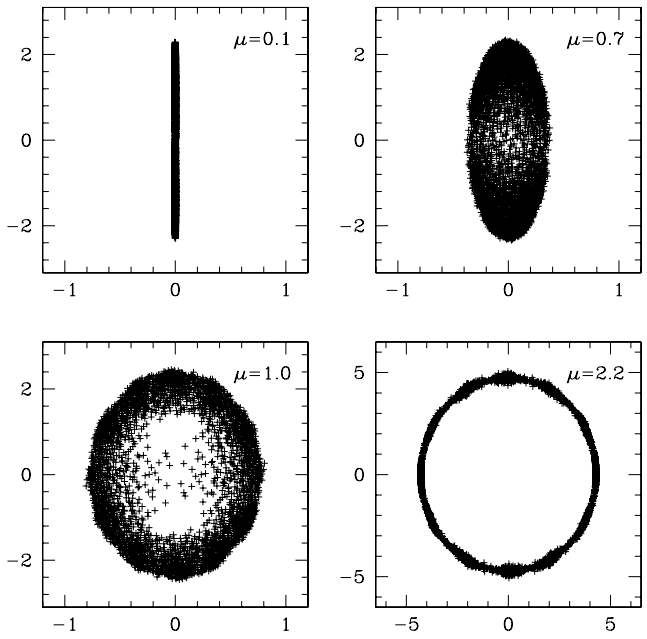

Figure 3. Scatter plot of the eigenvalues of the Dirac operator (in units of $1/a$) in the complex plane at various values of μ for a typical configuration of full QCD (generated at $\mu = 0$) in the confinement region at $\beta = 5.2$.

still very close to the Wigner distribution (1) whereas for $0.5 \leq \mu \leq 0.7$ ($\mu = 0.7$ not shown) we observe nice agreement with the Ginibre distribution (3). Values of μ in the crossover region between Wigner and Ginibre behavior ($0.1 < \mu < 0.3$) correspond to the regime of weak non-hermiticity mentioned above (the plots for $\mu = 0.3$ can be found in Ref. [12]). In this regime, the derivation of the spacing distribution is a very difficult problem, and the only known analytical result is $P(s, z_0)$ for small s, where z_0 is the location in the complex plane (i.e., no unfolding is performed) [14]. The small-s behavior of Eqs. (1) and (3) is given by $P_{\rm W}(s) \propto s^2$ and $P_{\rm G}(s) \propto s^3$, respectively, and in the regime of weak non-hermiticity we have $P(s, z_0) \propto s^\alpha$ (for $s \ll 1$) with $2 < \alpha < 3$ [14]. This smooth crossover from $\alpha = 2$ to $\alpha = 3$ is also observed in our unfolded data.

For $\mu > 0.7$ the lattice results for $P(s)$ deviate substantially from the Ginibre distribution. The global spectral density of the lattice data for $\mu = 1.0$ and 2.2 in Fig. 3 is very different from that of the Ginibre ensemble. This does not immediately imply that the local spectral fluctuations are also different, but it is an indication for qualitative changes. The results for $\mu = 2.2$ in Fig. 4 could be interpreted as Poisson behavior, corresponding

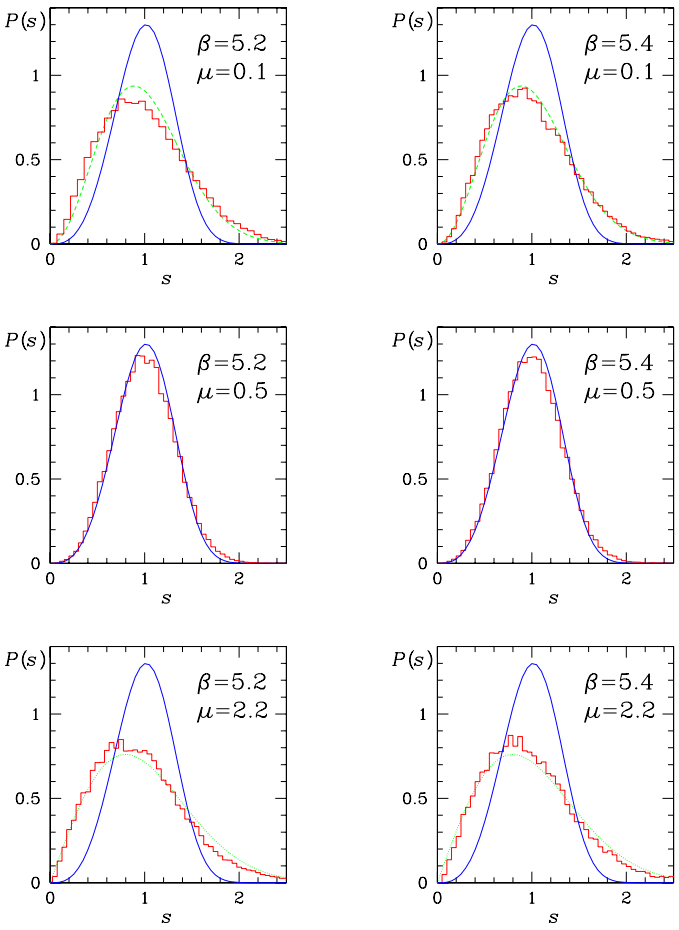

Figure 4. Nearest-neighbor spacing distribution of the Dirac operator eigenvalues in the complex plane for various values of μ in the confinement (left) and deconfinement (right) phase. The histograms represent the lattice QCD data. The solid curve is the Ginibre distribution of Eq. (3), the short-dashed curve in the first row the Wigner distribution of Eq. (1), and the dotted curve in the last row the Poisson distribution of Eq. (4).

to uncorrelated eigenvalues. (In the hermitian case at nonzero temperature, lattice simulations only show a transition to Poisson behavior for $\beta \to \infty$ when the physical box size shrinks and the theory becomes free [6].) A plausible explanation of the transition to Poisson behavior is provided by the following two (related) observations. First, for large μ the terms containing e^{μ} in Eq. (2) dominate the Dirac matrix, giving rise to uncorrelated eigenvalues. Second, for $\mu > 1.0$ the fermion density on the $6^3 \times 4$ lattice reaches saturation due to limited box size and the Pauli exclusion principle.

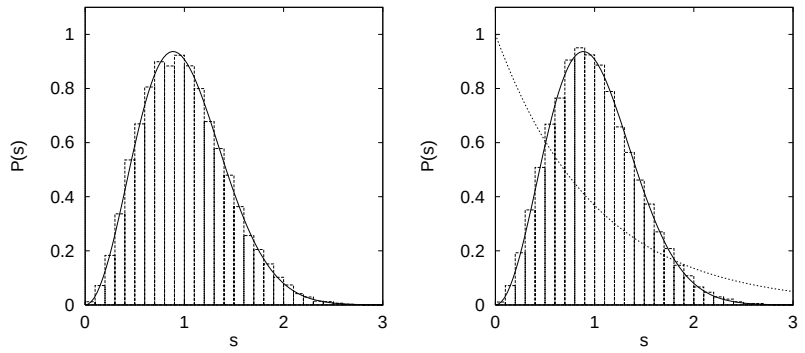

Figure 5. Nearest-neighbor spacing distribution $P(s)$ for U(1) gauge theory on an $8^3 \times 6$ lattice in the confined phase (left) and in the Coulomb phase (right). The theoretical curves are the chUE result, Eq. (1), and the Poisson distribution, $P_{\rm P}(s) = \exp(-s)$.

3. QED at Nonzero Temperature

By now it is a well-known fact that the spectrum of the QCD Dirac operator is related to universality classes of RMT, i.e., determined by the global symmetries of the QCD partition function. We have investigated 4d U(1) gauge theory which was not classified yet. At $\beta_c \approx 1.01$ U(1) gauge theory undergoes a phase transition between a confinement phase with mass gap and monopole excitations for $\beta < \beta_c$ and the Coulomb phase which exhibits a massless photon [18] for $\beta > \beta_c$. As for SU(2) and SU(3) gauge groups, we expect the confined phase to be described by RMT, whereas free fermions are known to yield the Poisson distribution (see Fig. 2). The question arose whether the Coulomb phase will be described by RMT or by the Poisson distribution [19]. The nearest-neighbor spacing distributions for an $8^3 \times 6$ lattice at $\beta = 0.9$ (confined phase) and at $\beta = 1.1$ (Coulomb phase), averaged over 20 independent configuration, are depicted in Fig. 5. Both are well described by the chiral unitary ensemble (chUE) of RMT.

We have continued the above investigation with a study of the distribution of small eigenvalues in the confined phase. The Banks-Casher formula [1] relates the eigenvalue density $\rho(\lambda)$ at $\lambda = 0$ to the chiral condensate, $\Sigma = |\langle\bar{\psi}\psi\rangle| = \lim_{m\to 0}\lim_{V\to\infty}\pi\rho(0)/V$. The microscopic spectral density, $\rho_s(z) = \lim_{V\to\infty}\rho\left(z/V\Sigma\right)/V\Sigma$, should be given by the result for the chUE of RMT [20]. This function also generates the Leutwyler-Smilga sum rules [21].

To study the smallest eigenvalues, spectral averaging is not possible, and one has to produce large numbers of configurations. Our present results are for $\beta = 0.9$ in the confined phase with 10000 configurations on a 4^4, 10000 configuration on a 6^4, and 2822 configurations on an $8^3 \times 6$ lattice. The left plot in Fig. 6 exhibits the distribution $P(\lambda_{\rm min})$ of the smallest eigenvalue

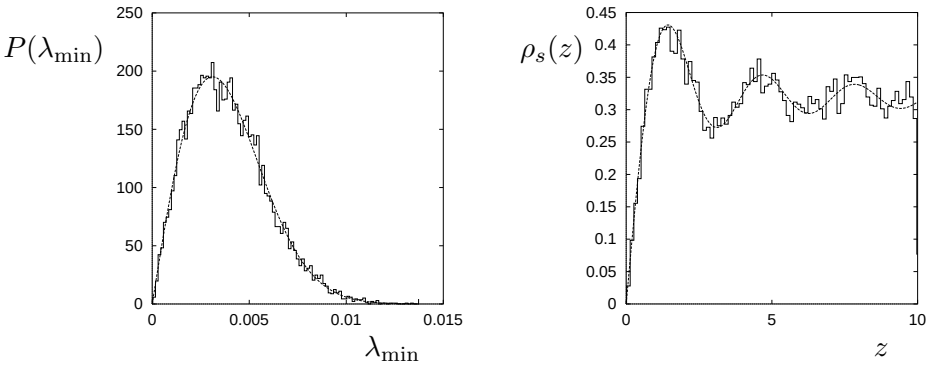

Figure 6. Distribution $P(\lambda_{\rm min})$ (left plot) and microscopic spectral density $\rho_s(z)$ (right plot) from our 6^4 lattice data of U(1) gauge theory in comparison with the predictions of the chUE of RMT (dashed lines).

$\lambda_{\rm min}$ in comparison with the prediction of the (quenched) chUE of RMT for topological charge $\nu = 0$,

$$P(\lambda_{\rm min}) = \frac{(V\Sigma)^2\lambda_{\rm min}}{2}\,\exp\left(-\frac{(V\Sigma\lambda_{\rm min})^2}{4}\right). \qquad (5)$$

The agreement is excellent for all lattices. For the chiral condensate we obtain $\Sigma \approx 0.35$ by extrapolating the histogram for $\rho(\lambda)$ to $\lambda = 0$ and using the Banks-Casher relation. Since the average value of $\lambda_{\rm min}$ goes like V^{-1}, $\langle\lambda_{\rm min}\rangle$ decreases with increasing lattice size. In the right plot of Fig. 6 the same comparison with RMT is done for the microscopic spectral density $\rho_s(z)$ up to $z = 10$, and the agreement is again quite satisfactory. Here, the analytical RMT result for the (quenched) chUE and $\nu = 0$ is given by [20] $\rho_s(z) = z\,[J_0^2(z) + J_1^2(z)]/2$, where J denotes the Bessel function.

The quasi-zero modes which are responsible for the chiral condensate $\Sigma \approx 0.35$ build up when we cross from the Coulomb into the confined phase. For our $8^3 \times 6$ lattice, Fig. 7 compares on identical scales densities of the small eigenvalues at $\beta = 0.9$ (left plot) and at $\beta = 1.1$ (right plot), averaged over 20 configurations. The quasi-zero modes in the left plot are related to the nonzero chiral condensate $\Sigma > 0$, whereas no such quasi-zero modes are found in the Coulomb phase. It may be worthwhile to understand the physical origin of the U(1) quasi-zero modes in more detail. For 4d SU(2) and SU(3) gauge theories a general interpretation is to link them, and hence the chiral condensate, to the existence of instantons. As there are no instantons in 4d U(1) gauge theory, one needs another explanation, and it is interesting to study local correlations of the fermion density with the topological charge density and the monopole density [22].

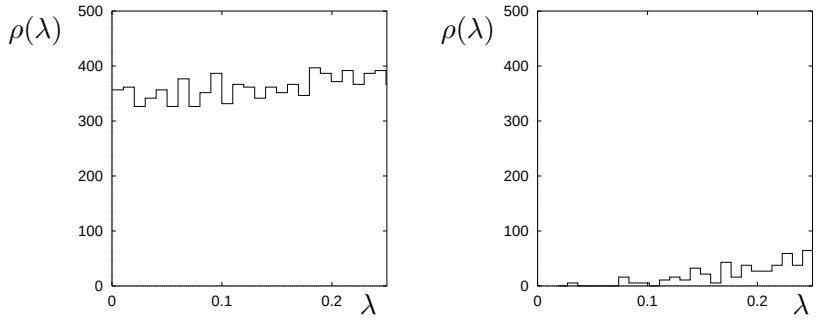

Figure 7. Density $\rho(\lambda)$ of small eigenvalues for the $8^3 \times 6$ lattice at $\beta = 0.9$ (left plot) and at $\beta = 1.1$ (right plot). A nonzero chiral condensate is supported in the confinement phase of U(1) gauge theory.

Another interesting question concerns the energy scale E_c up to which RMT describes the small Dirac eigenvalues in the phase where $\rho(0) > 0$. In disordered mesoscopic systems, a similar scale is called the Thouless energy. The theoretical prediction for QCD is $E_c \sim f_\pi^2/\Sigma L_s^2$ [23] with the pion decay constant f_π, where we have assumed that the spatial extent L_s of the lattice is not smaller than the temporal extent L_t. In units of the mean level spacing $\Delta = \pi/V\Sigma$ at the origin, this becomes

$$u_c \equiv \frac{E_c}{\Delta} \sim \frac{1}{\pi} f_\pi^2 L_s L_t \; . \tag{6}$$

A convenient quantity from which u_c can be extracted is the disconnected scalar susceptibility,

$$\chi_{\rm latt}^{\rm disc}(m) = \frac{1}{N} \left\langle \sum_{k,l=1}^{N} \frac{1}{(i\lambda_k + m)(i\lambda_l + m)} \right\rangle_A - \frac{1}{N} \left\langle \sum_{k=1}^{N} \frac{1}{i\lambda_k + m} \right\rangle_A^2 . \tag{7}$$

The corresponding RMT result for the quenched chUE with $\nu = 0$ reads [24] $\chi_{\rm RMT}^{\rm disc} = u^2[K_1^2(u) - K_0^2(u)][I_0^2(u) - I_1^2(u)]$, where $u = mV\Sigma$, and I and K are modified Bessel functions. In Fig. 8 we have plotted the ratio [25]

$$\text{ratio} = \left(\chi_{\rm latt}^{\rm disc} - \chi_{\rm RMT}^{\rm disc}\right) / \chi_{\rm RMT}^{\rm disc} \tag{8}$$

versus u and $u/(L_s L_t)$, respectively, for the U(1) data computed at $\beta = 0.9$. This ratio should deviate from zero above the Thouless scale. The expected scaling of the Thouless energy with $L_s L_t$ is confirmed.

4. Conclusions

We have searched for a transition in the nearest-neighbor spacing distribution $P(s)$ from Wigner to Poisson behavior across the deconfinement phase

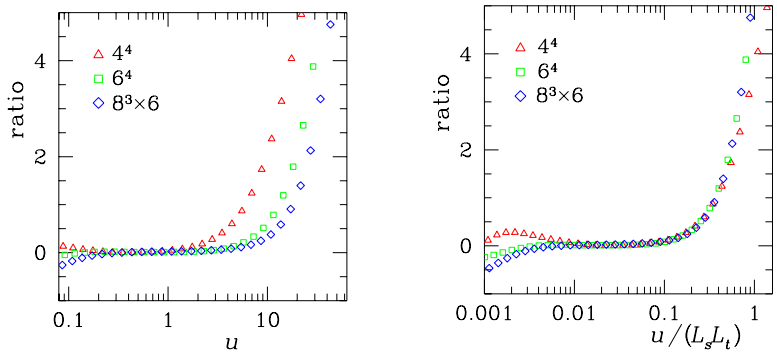

Figure 8. The ratio of Eq. (8) for U(1) gauge theory plotted versus u and $u/(L_s L_t)$, respectively (error bars not shown). In the right plot, the data for different L_s and L_t fall on the same curve, confirming the expected scaling of the Thouless energy according to Eq. (6). The deviations of the ratio from zero for very small values of u are well-understood artifacts of the finite lattice size and finite statistics [25].

transition of pure gluonic and of full QCD. We observed no signature of a transition, neither for pure SU(3) nor for full QCD. The data agree with the RMT result in both phases, except for extremely large values of β where the eigenvalues are known analytically. Our analysis of full QCD shows that quark masses have no influence on the nearest-neighbor spacing distribution. One explanation of our results is that temporal monopole currents survive the deconfinement phase transition leading to confinement of spatial Wilson loops. Thus, even in the deconfinement phase, the gauge fields retain a considerable degree of randomness.

A general unfolding procedure for the spectra of non-hermitian operators was applied to the QCD lattice Dirac operator at nonzero chemical potential. Agreement of the nearest-neighbor spacing distribution with predictions of the Ginibre ensemble of non-hermitian RMT was found between $\mu = 0.5$ and $\mu = 0.7$ in both confinement and deconfinement phase. The deviations from Ginibre behavior for smaller values of μ as well as the changes for larger values of μ toward a Poisson shape are understood mathematically. The physical interpretation requires a better understanding of QCD at nonzero density. An interesting observation is that the results for $P(s)$ in the non-hermitian case are rather sensitive to μ whereas they are very stable under variations of T in the hermitian case.

The nearest-neighbor spacing distribution of 4d U(1) quenched lattice gauge theory is described by the chUE in both the confinement and the Coulomb phase. In the confinement phase we also find that the $P(\lambda_{\rm min})$ distribution and the microscopic spectral density $\rho_s(z)$ are described by the chUE. The Thouless energy scales with the lattice size as expected.

5. Acknowledgments

This work was supported in part by FWF projects P10468-PHY and P11456-PHY, by DFG grants We 655/11-2 and We 655/15-1, by DOE contracts DE-FG02-97ER41022, DE-FG05-85ER2500, and DE-FG02-91ER40608, and by the RIKEN BNL Research Center. We thank T.S. Biró, E.-M. Ilgenfritz, N. Kaiser, M.I. Polikarpov, K. Rabitsch, and J.J.M. Verbaarschot for helpful discussions.

References

1. T. Banks and A. Casher, Nucl. Phys. B 169 (1980) 103.
2. M.A. Halasz and J.J.M. Verbaarschot, Phys. Rev. Lett. 74 (1995) 3920; M.A. Halasz, T. Kalkreuter, and J.J.M. Verbaarschot, Nucl. Phys. B (Proc. Suppl.) 53 (1997) 266.
3. O. Bohigas, M.-J. Giannoni, and C. Schmit, Phys. Rev. Lett. 52 (1984) 1.
4. J.J.M. Verbaarschot, Phys. Rev. Lett. 72 (1994) 2531.
5. D. Fox and P.B. Kahn, Phys. Rev. 134 (1964) B1151; T. Nagao and M. Wadati, J. Phys. Soc. Jpn. 60 (1991) 3298; 61 (1992) 78; 61 (1992) 1910.
6. R. Pullirsch et al., Phys. Lett. B 427 (1998) 119.
7. M.L. Mehta, *Random Matrices*, 2nd ed. (Academic Press, San Diego, 1991).
8. M.A. Stephanov, Phys. Rev. Lett. 76 (1996) 4472.
9. P. Hasenfratz and F. Karsch, Phys. Lett. B 125 (1983) 308; I.M. Barbour, Nucl. Phys. B (Proc. Suppl.) 26 (1992) 22.
10. M.A. Halasz, J.C. Osborn, and J.J.M. Verbaarschot, Phys. Rev. D 56 (1997) 7059.
11. R. Grobe, F. Haake, and H.-J. Sommers, Phys. Rev. Lett. 61 (1988) 1899.
12. H. Markum, R. Pullirsch, and T. Wettig, Phys. Rev. Lett. 83 (1999) 484.
13. J. Ginibre, J. Math. Phys. 6 (1965) 440.
14. Y.V. Fyodorov and H.-J. Sommers, JETP Lett. 63 (1996) 1026; J. Math. Phys. 38 (1997) 1918; Y.V. Fyodorov, B.A. Khoruzhenko, and H.-J. Sommers, Phys. Lett. A 226 (1997) 46; Phys. Rev. Lett. 79 (1997) 557.
15. I.M. Barbour et al., Phys. Rev. D 56 (1997) 7063.
16. M.A. Halasz, A.D. Jackson, and J.J.M. Verbaarschot, Phys. Rev. D 56 (1997) 5140.
17. I. Barbour et al., Nucl. Phys. B 275 (1986) 296.
18. B.A. Berg and C. Panagiotakopoulos, Phys. Rev. Lett. 52 (1984) 94.
19. B.A. Berg, H. Markum, and R. Pullirsch, Phys. Rev. D 59 (1999) 097504.
20. E.V. Shuryak and J.J.M. Verbaarschot, Nucl. Phys. A 560 (1992) 306; J.J.M. Verbaarschot and I. Zahed, Phys. Rev. Lett. 70 (1993) 3852; J.C. Osborn, D. Toublan, and J.J.M. Verbaarschot, Nucl. Phys. B 540 (1999) 317; P.H. Damgaard et al., Nucl. Phys. B 547 (1999) 305.
21. H. Leutwyler and A.V. Smilga, Phys. Rev. D 46 (1992) 5607.
22. W. Sakuler, S. Thurner, and H. Markum, Phys. Lett. B 464 (1999) 272.
23. J.C. Osborn and J.J.M. Verbaarschot, Nucl. Phys. B 525 (1998) 738; Phys. Rev. Lett. 81 (1998) 268; R.A. Janik et al., Phys. Rev. Lett. 81 (1998) 264.
24. M. Göckeler et al., Phys. Rev. D 59 (1999) 094503.
25. M.E. Berbenni-Bitsch et al., Phys. Lett. B 438 (1998) 14.